Frequency based design of modal controllers for adaptive optics systems

Frequency based design of modal controllers for adaptive optics systems

Guido Agapito,[1] **Giorgio Battistelli,**[2] **Daniele Mari,**[2] **Daniela Selvi,**[2,*] **Alberto Tesi,**[2] **and Pietro Tesi**[3]

[1]*Osservatorio Astrofisico di Arcetri, Largo E. Fermi 5, Firenze, Italy*
[2]*Dipartimento Sistemi e Informatica, DSI, University of Florence, Via S. Marta 3, 50139 Firenze, Italy*
[3]*DIBRIS, University of Genoa, Via Opera Pia 13, 16145 Genova, Italy*
**daniela.selvi@unifi.it*

Abstract: This paper addresses the problem of reducing the effects of wavefront distortions in ground-based telescopes within a "Modal-Control" framework. The proposed approach allows the designer to optimize the Youla parameter of a given modal controller with respect to a relevant adaptive optics performance criterion defined on a "sampled" frequency domain. This feature makes it possible to use turbulence/vibration profiles of arbitrary complexity (even empirical power spectral densities from data), while keeping the controller order at a moderate value. Effectiveness of the proposed solution is also illustrated through an adaptive optics numerical simulator.

OCIS codes: (010.1080) Adaptive optics; (010.1330) Atmospheric turbulence; (999.9999) Optimal control.

References and links

1. F. Roddier, *Adaptive Optics in Astronomy* (Cambridge University Press, 1999).
2. C. Kulcsár, H.-F. Raynaud, C. Petit, J.-M. Conan, and P. Viaris de Lesegno, "Optimal control, observers and integrators in adaptive optics," Opt. Express **14**(17), 7464–7476 (2006).
3. C. Petit, J.-M. Conan, C. Kulcsár, H.-F. Raynaud, and T. Fusco, "First laboratory validation of vibration filtering with LQG control law for adaptive optics," Opt. Express **16**(1), 87–97 (2008).
4. E. Fedrigo, R. Muradore, and D. Zillo, "High performance adaptive optics system with fine tip/tilt control," Control Eng. Pract. **17**(1), 122–135 (2009).
5. L.A. Poyneer, B.A. Macintosh, and J.-P. Véran, "Fourier transform wavefront control with adaptive prediction of the atmosphere," J. Opt. Soc. Am. A, **24**(9), 2645–2660 (2007).
6. K. Hinnen, M. Verhaegen, and N. Doelman, "A data-driven H_2-optimal control approach for adaptive optics," IEEE Trans. Control Syst. Technol, **16**(3), 381–395 (2008).
7. "Adaptive optics control for ground based telescopes," in *Special Issue of the European Journal of Control*, *Vol*. 17, *No*. 3, J.-M. Conan, C.Kulcsár, and H.-F. Raynaud, eds. (Lavoisier, 2011).
8. G. Agapito, F. Quiros-Pacheco, P. Tesi, A. Riccardi, and S. Esposito, "Observer-based control techniques for the LBT adaptive optics under telescope vibrations," Eur. J. Control **17**(3), 316–326 (2011).
9. G. Agapito, S.Baldi, G.Battistelli, D.Mari, E.Mosca, and A.Riccardi, "Automatic tuning of the internal position control of an adaptive secondary mirror," Eur. J. Control **17**(3), 273–289 (2011).
10. G. Agapito, F. Quiros-Pacheco, P. Tesi, S. Esposito, and M. Xompero, "Optimal control techniques for the adaptive optics system of the LBT," Proc. SPIE **7015**, 70153G (2008).
11. L. Close, V. Gasho, D. Kopon, J. Males, K.B. Follette, K. Brutlag, A. Uomoto, and T. Hare, "The Magellan telescope adaptive secondary AO system: a visible and mid-IR AO facility," Proc. SPIE **7736,** 773605 (2010).
12. E. Marchetti, M. Le Louarn, C. Soenke, E. Fedrigo, P.-Y. Madec, and N. Hubin, "ERIS adaptive optics system design," Proc. SPIE **8447,** 84473M (2012).

#173695 - $15.00 USD Received 2 Aug 2012; revised 12 Oct 2012; accepted 14 Oct 2012; published 16 Nov 2012

13. S. Esposito, E. Pinna, F. Quirós-Pacheco, A. Puglisi, L. Carbonaro, M. Bonaglia, V. Biliotti, R. Briguglio, G. Agapito, C. Arcidiacono, L. Busoni, M. Xompero, A. Riccardi, L. Fini, and A. Bouchez, "Wavefront sensor design for the GMT natural guide star AO system," Proc. SPIE **8447,** 84471L (2012) .
14. M. Born and E. Wolf, *Principles of Optics* (Cambridge University Press, Cambridge, U.K, 1980).
15. C. Dessenne, P.-Y. Madec, and G. Rousset, "Optimization of a predictive controller for closed-loop adaptive optics," Appl. Optim., **37**(21), 4623-4633 (1998).
16. E. Gendron and P. Lena, "Modal control optimization," Astron. Astrophys., **291**, 337-347 (1994).
17. C. Petit, F. Quiros-Pacheco, J.-M. Conan, C. Kulcsár, H.-F. Raynaud, T. Fusco, and G. Rousset, "Kalman filter based control for adaptive optics," Proc. SPIE **5490**, 1414–1425 (2004).
18. C.Correia, H.F.Raynaud, C.Kulcsar, and J.M.Conan, "Minimum-variance control for astronomical adaptive optics with resonant deformable mirrors," Eur. J. Control **17**(3), 222–236 (2011).
19. D. P. Looze, M. Kasper, S. Hippler, O. Beker, and R. Weiss, "Optimal compensation and implementation for adaptive optics systems," Exp. Astron., **15,** 67–88 (2004).
20. L. A. Poyneer, and J.-P. Véran, "Optimal modal Fourier transform wavefront control," J. Opt. Soc. Am. A, **22**(2), 1515–1526 (2005).
21. B. Le Roux, J.-M. Conan, C. Kulcsár, H.-F. Raynaud, L. Mugnier, and T. Fusco, "Optimal control law for classical and multiconjugate adaptive optics," J. Opt. Soc. Am. A, **21**(7), 1261-1276 (2004).
22. A. Riccardi, G. Brusa, P. Salinari, D. Gallieni, R. Biasi, M. Andrighettoni, and H. M. Martin, "Adaptive secondary mirrors for the Large Binocular Telescope," Proc. SPIE **4839**, 721–732 (2003).
23. J. Herrmann, "Phase variance and Strehl ratio in adaptive optics," J. Opt. Soc. Am. A, **9,** 2257–2258 (1992).
24. R.A. de Callafon and C.E. Kinney, "Robust estimation and adaptive controller tuning for variance minimization in servo systems," JSME J. Adv. Mech. Des. Syst. Manuf., **4**(1), 130-142 (2010).
25. J. Doyle, B. Francis, and A. Tannenbaum, *Feedback Control Theory* (Macmillan Publishing Company, 1992).
26. A. Karimi and G. Galdos, "Fixed-order H_∞ controller design for nonparametric models by convex optimization," Automatica **46**, 1388–1394 (2010).
27. G. Goodwin, S. Graebe, and M. Salgado, *Control System Design* (Prentice Hall, 2001).
28. R. Ragazzoni, "Pupil plane wavefront sensing with an oscillating prism," J. Mod. Optic. **43**, 289–293 (1996).
29. C. Vérinaud, "On the nature of the measurements provided by a pyramid wave-front sensor," Opt. Commun. **233**(1–3), 27 – 38 (2004).
30. B. L. McGlamery, "Computer simulation studies of compensation of turbulence degraded images," Proc. SPIE, **74**(9), 225–233 (1976).

1. Introduction

A central problem when dealing with ground-based telescopes arises from deformations on the light wavefront caused by the atmosphere. It is well known that the maximum resolution of any optical device is due to diffraction; in order to recover diffraction limited resolution, modern ground-based telescopes are equipped with adaptive optics (AO) devices, which aim at reducing, thanks to the use of deformable mirrors, the aforementioned effects of wavefront distortion. In addition to the atmospheric turbulence [1], telescopes also suffer from structural vibrations due to situations such as telescope orientation, telescope tracking errors, and wind shaking. Due to their potential impact, considerable attention has been devoted over the last decades to the analysis and design of AO systems. Together with developments of physics, mathematics and technology, contributions to the subject have been recently proposed also from a control engineering perspective, as witnessed by [2–6] and the special issue on AO for ground-based telescopes organized by the European Journal of Control [7].

In this work, we focus on the control architecture installed on the Large Binocular Telescope (LBT, located on Mt. Graham, Arizona, USA) [8–10], and one of the two Magellan Telescopes (Las Campanas Observatory, Chile) [11]. A similar architecture will be also adopted for the upgrading of one of the four Very Large Telescopes (Cerro Paranal, Chile) [12] and the Giant Magellan Telescope (Las Campanas, Chile), which is expected to be operative by the end of 2024 [13]. The considered AO unit comprises a wavefront sensor (WFS) - in this work a pyramid one has been taken into account - an adaptive secondary mirror (ASM), and a real-time computer (RTC). Roughly speaking, the pyramid WFS delivers a signal that is proportional, by a first-order approximation, to the first derivative of the incoming wavefront. The RTC, which implements the AO controller, computes the command vector driving the actuators of the ASM.

#173695 - $15.00 USD Received 2 Aug 2012; revised 12 Oct 2012; accepted 14 Oct 2012; published 16 Nov 2012

Through the use of hundreds of voice-coil (electro-magnetic force) actuators, distributed on the mirror shell, the ASM corrects the wavefront distortion according to the RTC command vector. The correction is realized in such a way that the shape of the shell of the ASM becomes, as closely as possible, opposite to that of the wavefront distortion [1, 14].

Classic approaches to AO control can be subdivided into two main groups: those which do not employ any form of identification of turbulence and vibrations models [15, 16]; and those which employ models of turbulence and/or vibrations in combination with model-based control design techniques, such as H_2, H_∞ and LQG control. [2, 3, 8, 17, 18]. Model-based approaches have the intuitive advantage of including a notion of *optimality* in the sense of performance (Strehl ratio) ideally achievable for the identified process model. Achieving an exact modelling of turbulence and vibrations is however a practically impossible task, *i.e.* models will necessarily be approximate. It is therefore important that the models used to synthesize the controller are sufficiently accurate at the frequencies of concern. Herein lies the difficulty: model-based approaches provide controllers whose order is essentially determined by the order of the underlying models. High-order turbulence/vibrations models, in addition to requiring non-negligible identification effort, will therefore lead to high-order controllers, which may be infeasible (or simply not desired) from an implementation viewpoint. On the other hand, models with reduced complexity may fail to capture well the behavior of turbulence and/or vibrations at the frequencies of concern.

In this paper, we describe an approach which can moderate the aforementioned difficulties within a "Modal-Control" framework [4, 8, 18–21]. Specifically, it allows to optimize the parameters of a modal controller of given order with respect to a relevant AO performance criterion which is defined on a "sampled" frequency-domain. By sampled frequency-domain we mean that the optimization procedure involves samples of turbulence and vibrations frequency profiles, rather than their analytical models (as happens in classical H_2, H_∞ and LQG control design). This makes it possible to use turbulence/vibration profiles of arbitrary complexity, even empirical power spectral densities (PSDs) from data, while keeping the controller order at a desired (manageable) value. As elaborated next in detail, the proposed approach relies on the idea of optimizing the Youla parameter starting from a given stabilizing controller which can be either: i) a non-model-based controller, avoiding any identification effort; or ii) a model-based (H_2, H_∞ or alike) controller synthesized in accordance with turbulence and vibration models of limited complexity, avoiding to identify mathematical models of turbulence and vibrations of increased complexity. Because of this, the proposed approach is best viewed as cooperative with (rather than as alternative to) other control design approaches. Also, the problem can be cast as a quadratic programming problem (unconstrained, or with linear constraints if the controller is required to be stable), which can be efficiently solved by means of standard optimization routines.

The remainder of the paper is as follows. Section 2 describes the problem from a control perspective, along with the control system architecture. Sections 3 and 4 are devoted to the explanation of the proposed control synthesis strategy, with particular emphasis on the choice of the class of controllers and the description of the optimization problem to be solved. Simulation results are presented in Section 5 using an End-to-End Simulator for the performance analysis of the First Light Adaptive Optics (FLAO) system of the LBT. Finally, concluding remarks are provided in Section 6.

2. AO control system architecture

The architecture of the AO control system we consider is depicted in Fig. 1, and is composed of an *external* AO control system (working at the AO sampling time $T_s = 1$ ms), whose task is to determine the commands to the ASM, and an *internal* ASM control system (with sampling time

#173695 - $15.00 USD Received 2 Aug 2012; revised 12 Oct 2012; accepted 14 Oct 2012; published 16 Nov 2012

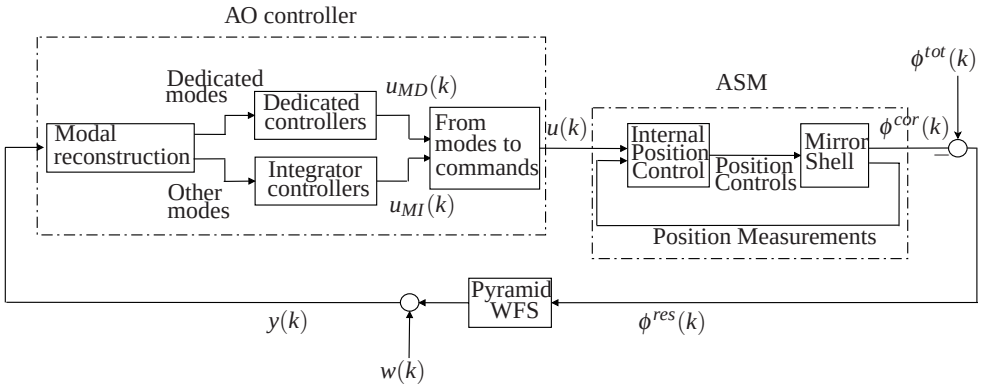

Fig. 1. AO control scheme.

$T_{ASM} \approx 10^{-2} T_s$). The principal devices characterizing the control loop are the AO controller, the Pyramid WFS, and the ASM. The AO controller receives at time kT_s the measurement vector $y(k) \in \mathbb{R}^q$, with q the number of measurements, from the Pyramid WFS and computes the command vector $u(k) \in \mathbb{R}^p$, with p the number of actuators, so as to pilot the actuators acting on the ASM shell. The command vector provides the information about the shape to be reproduced by the shell in order to compensate for the wavefront distortions. Due to the non-negligible dynamics of the shell, a dedicate control loop is needed to get the desired shape within T_s. Such a control loop is realized through the use of p capacitive sensors co-located with the actuators and placed at the back of the shell. Specifically, the control law piloting each actuator has a decentralized component obtained by a Proportional-Derivative feedback action which depends on the measurement of the co-located sensor, and a centralized component implemented through a feed-forward action which equals the force needed to statically deform the shell as indicated by the command vector $u(k)$: this latter action is obtained by multiplying $u(k)$ with the estimate of a shell stiffness matrix of dimensions $p \times p$, which is a-priori calibrated. For more details about the ASM internal position control, the interested reader is referred to [9, 22].

In Fig. 1 the phase aberration of the light wavefront due to turbulence and vibrations is denoted by $\phi^{tot}(k)$. Such a distortion has to be corrected by the shell deformations which provide the so called correction phase $\phi^{cor}(k)$. The difference $\phi^{res}(k) = \phi^{tot}(k) - \phi^{cor}(k)$ is the residual phase after the ASM correction. The objective of the external control loop therefore consists in regulating the residual phase $\phi^{res}(k)$ about 0.

The control architecture of Fig. 1 refers to a modal control scheme where the phase aberrations are expressed through a modal basis. Common choices in this regard are *Zernike* and *Karhunen-Loève* basis [1, 14], the latter being considered in this paper. The residual phase is translated into the measurement vector $y(k)$ from the Pyramid WFS as described by the following

$$y(k) = \mathscr{D}\,\phi^{res}(k-1) + w(k)\,, \tag{1}$$

where $w(k) \in \mathbb{R}^q$ is the measurement noise vector, which can be assumed to be a zero-mean white noise. The matrix $\mathscr{D}$ characterizes the WFS and describes the geometric relationship between the modal space and the measurement space. Notice that the modal space depends on the selected modal basis and all the phase variables represent coefficient vectors belonging to $\mathbb{R}^p$, where p denotes the dimension of the modal space.

The ASM correction phase is obtained as

$$\phi^{cor}(k) = \mathscr{N}\,u(k-1), \tag{2}$$

#173695 - $15.00 USD Received 2 Aug 2012; revised 12 Oct 2012; accepted 14 Oct 2012; published 16 Nov 2012

where $\mathscr{N}$ is the so-called *Commands-to-Modes* matrix, which describes the geometric relationship between the command space and the modal space. An estimate of $\mathscr{N}$ can be obtained via finite elements analysis of the mirror shell, once chosen the modal basis to be used.

The command vector provided to the ASM is computed by the AO controller as follows

$$U(z) = \mathscr{M}\,\mathscr{K}_M(z)\mathscr{R}Y(z)\,, \tag{3}$$

where $U(z)$ and $Y(z)$ are the Z-transforms of $u(k)$ and $y(k)$, respectively (hereafter we will use the corresponding capital letter to denote the Z-transform of a lower-case letter signal). $\mathscr{M}$ is the *Modes-to-Commands* (or *Projection*) matrix, represented by the *From modes to commands* block in Fig. 1, and $\mathscr{R}$ is the *Reconstruction* matrix, which yields the geometric relationship between the WFS measurements and the deformations of the ASM (*Modal reconstruction* block in Fig. 1). The transfer matrix $\mathscr{K}_M(z)$ has dimension $p \times p$ and has to be designed in order to satisfy the control requirements. In the proposed setting, $\mathscr{K}_M(z)$ is chosen as a diagonal matrix, $\mathscr{K}_M(z) = \mathrm{diag}\{C_1(z), \cdots, C_p(z)\}$, as the ideal goal would be to control the $i-$th mode by means of controller $C_i(z)$.

In fact, the residual phase satisfies the relationship

$$\mathbf{\Phi}^{res}(z) = \mathbf{\Phi}^{tot}(z) - \mathscr{N}\,z^{-1}U(z) = \mathbf{\Phi}^{tot}(z) - \mathscr{N}\,z^{-1}\,\mathscr{M}\,\mathscr{K}_M(z)\mathscr{R}Y(z) \tag{4}$$

which can be rewritten as

$$\Delta(z)\,\mathbf{\Phi}^{res}(z) = \mathbf{\Phi}^{tot}(z) - \Xi(z)\,W(z) \tag{5}$$

where $\Delta(z) := (I + z^{-2}\mathscr{N}\,\mathscr{M}\,\mathscr{K}_M(z)\mathscr{R}\,\mathscr{D})$ and $\Xi(z) := z^{-1}\,\mathscr{N}\,\mathscr{M}\,\mathscr{K}_M(z)\mathscr{R}$. The matrix $\mathscr{R}$ is then selected as the Moore-Penrose inverse of $\mathscr{D}$, *i.e.* $\mathscr{R} := (\mathscr{D}^T\mathscr{D})^{-1}\mathscr{D}^T$. Accordingly, $\Delta(z)$ simplifies to $\Delta(z) = (I + z^{-2}\mathscr{N}\,\mathscr{M}\,\mathscr{K}_M(z))$. The matrices $\mathscr{N}$ and $\mathscr{M}$ are instead calibrated so as to yield $\mathscr{N}\,\mathscr{M} \approx I$ (more precisely for the LBT, $\mathscr{N}\,\mathscr{M}$ is a matrix with elements on the diagonal equal to 1 and extra-diagonal elements with absolute values $\approx 2^{-15}$). Thus, by neglecting the measurement noise, we can therefore select a diagonal controller $\mathscr{K}_M(z)$ and achieve modal decoupling, *i.e.* $\mathbf{\Phi}^{res}(z) \approx (I + z^{-2}\mathscr{K}_M(z))^{-1}\,\mathbf{\Phi}^{tot}(z)$.

In principle, one could synthesize a dedicated controller $C_i(z)$ for each mode. However, in practice, it is convenient to consider advanced control design techniques only for those modes having more influence on the value of $\mathbf{\Phi}^{res}(k)$. Within the addressed framework, a dedicated controller $C_D(z)$ is synthesized only for tip and tilt modes [4, 8, 10], which consist in the image displacements in the two orthogonal directions of the focal plane, while the remaining modes are regulated by simple integrator controllers $C_I(z) = gz/(z-1)$, where g is a gain to be set. In fact, it has been observed by means of experimental studies on LBT that turbulence and vibrations affect mainly tip/tilt modes. In turn, the experimental studies have revealed that in the considered operating setting tip/tilt modes yield more than 80% of the overall atmospheric turbulence variance. The choice of considering only two dedicated controllers has been mainly motivated by the memory constraints of the RTC which, as detailed in [8], has been designed to work with a modal integrator, so that the maximum state dimension allowed for the AO controller $\mathscr{K}_M(z)$ is 672. It is however important to point out that the design procedure proposed in the following sections is well-suited to being applied to each modal controller $C_i(z)$.

Let $u_M(k) \in \mathbb{R}^p$ be the command vector in the modal space, such that $u(k) = \mathscr{M}\,u_M(k)$, and suppose that tip and tilt correspond to the first two entries of the vector $u_M(k)$, then $\mathscr{K}_M(z) = diag\{C_D(z), C_D(z), C_I(z), \cdots, C_I(z)\}$, where for simplicity the same controller is used for tip and tilt modes. In the sequel, for notation simplicity, we simply write $C(z)$ instead of $C_D(z)$. In addition, with reference to control scheme of Fig. 2, we adopt the subscript "t" to indicate variables related to tip/tilt modes.

#173695 - $15.00 USD Received 2 Aug 2012; revised 12 Oct 2012; accepted 14 Oct 2012; published 16 Nov 2012

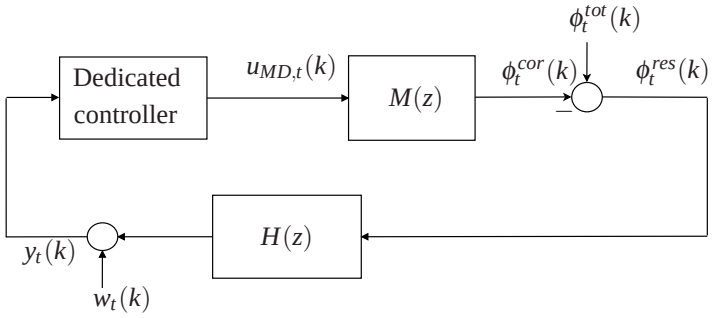

Fig. 2. Modal control scheme.

3. Modal control design: a frequency based approach

Let $C(z,\rho)$ represent the transfer function of an arbitrary controller with fixed structure depending on a parameter vector ρ which has to be tuned so as to achieve the desired performance, where the choice of $C(z,\rho)$ will be discussed more accurately in the sequel of the section. Hereafter, we will denote by $P(z)$ the transfer function of the plant to be controlled through $C(z,\rho)$. By referring to Fig. 2, $P(z)$ consists of the cascade of the blocks $M(z)$ and $H(z)$, representing the dynamics of the ASM and WFS, respectively. It is to be pointed out that, within our setting, both $M(z)$ and $H(z)$ can be assumed to behave as a unit delay, in that their tasks are executed within one sampling time of the external loop. Specifically, the internal position control acting on the mirror shell, see Fig. 1, works with a sampling time much lower than the one of the external AO loop (in LBT, for example, it is about 0.01 ms), and thus it allows the mirror shell to achieve the desired shape within one AO loop sampling time. Accordingly, we can assume $M(z) = 1/z$ and $H(z) = 1/z$.

The main objective of the AO system is to regulate the residual phase about zero by rejecting the disturbances acting on the system. To this end, a typical AO performance criterion to be minimized is the sampled-valued variance of the residual phase, defined as (see [18])

$$f(\rho) = \lim_{h\to\infty} \frac{1}{h+1} \sum_{k=0}^{h} |\phi_t^{res}(k)|^2 . \tag{6}$$

In fact, minimizing $f(\rho)$ amounts to maximizing the Strehl-ratio (SR), which is the ratio of the maximum of the Point Spread Function (PSF) of the distorted image and the maximum of the theoretical diffraction limited image PSF [23]. Let now $\Upsilon_\phi(\omega)$ and $\Upsilon_w(\omega)$ denote the PSDs of the signals $\phi_t^{tot}(k)$ and $w_t(k)$, respectively. Supposing $\phi_t^{tot}(k)$ and $w_t(k)$ mutually uncorrelated, by virtue of the Parseval's relationship, one can rewrite $f(\rho)$ in the frequency domain as follows

$$f(\rho) = \frac{1}{2\pi} \int_{-\pi}^{\pi} (|S(e^{j\omega},\rho)|^2 \Upsilon_\phi(\omega) + |T(e^{j\omega},\rho)|^2 \Upsilon_w(\omega)) d\omega , \tag{7}$$

where $S(z,\rho)$, called the sensitivity function, is the transfer function mapping the phase aberration $\phi_t^{tot}(k)$ into the residual phase $\phi_t^{res}(k)$, whereas $T(z,\rho)$ is the transfer function mapping the measurement noise $w_t(k)$ into the residual phase $\phi_t^{res}(k)$. With reference to Fig. 2, it is immediate to see that $S(z,\rho) = (1+C(z,\rho)P(z))^{-1}$ and $T(z,\rho) = -M(z)C(z,\rho)(1+C(z,\rho)P(z))^{-1}$.

In practice, it is convenient to approximate the integral in Eq. (7) with a finite sum by considering the samples at certain frequencies $\omega_1, \omega_2, \ldots, \omega_N$ of the PSDs of $\phi_t^{tot}(k)$ and $w_t(k)$. These samples can be obtained either from a model, possibly infinite-dimensional and non parametric,

#173695 - $15.00 USD Received 2 Aug 2012; revised 12 Oct 2012; accepted 14 Oct 2012; published 16 Nov 2012

or directly from collected data series. Accordingly, we redefine the performance criterion in Eq. (7) as

$$f(\rho) = \frac{1}{N}\sum_{f=1}^{N}\left(|S(e^{j\omega_f},\rho)|^2\,\hat{\Upsilon}_\phi(\omega_f) + |T(e^{j\omega_f},\rho)|^2\,\hat{\Upsilon}_w(\omega_f)\right), \tag{8}$$

where $\hat{\Upsilon}_\phi(\omega_f)$ and $\hat{\Upsilon}_\phi(\omega_f)$ denote estimates of the PSDs $\Upsilon_\phi(\omega_f)$ and $\Upsilon_\phi(\omega_f)$, respectively, at the frequency ω_f.

In order to derive a controller $C(z,\rho)$ with optimized performance with respect to the objective function $f(\rho)$, we resort to the well-known *Youla* parametrization [24]. In particular, let $\mathscr{S}$ be the family of all the proper transfer functions with poles inside the open unit disk, and $\mathscr{C}(P)$ the set of all stabilizing controllers, i.e., the set of all controllers which are able to guarantee that the closed-loop is internally stable. Since $P(z) \in \mathscr{S}$, the set of all stabilizing controllers takes the form ([25], Chapter 5)

$$\mathscr{C}(P) = \left\{ C(z) = \frac{Q(z)}{1 - P(z)\,Q(z)}, \qquad Q(z) \in \mathscr{S} \right\}, \tag{9}$$

where $Q(z)$, the so-called *Youla parameter*, is an arbitrary transfer function belonging to $\mathscr{S}$. It is straightforward to prove that the controllers which can be expressed as shown in Eq. (9) are all and the only ones which guarantee the internal stability ([25], Chapter 5).

We point out that the transfer function $Q(z)$ has to be regarded as a free parameter which can be tuned so as to achieve the desired control performance. To this end, we give $Q(z)$ a fixed structure depending on a parameter vector ρ, i.e., $Q(z) = Q(z,\rho)$, thus considering controllers of the form

$$C(z,\rho) = \frac{Q(z,\rho)}{1 - P(z)\,Q(z,\rho)}. \tag{10}$$

One of the main positive features of the Youla parametrization is that it allows one to express both $S(z,\rho)$ and $T(z,\rho)$ in a form which is affine in the Youla parameter $Q(z,\rho)$ in that

$$S(z,\rho) = 1 - P(z)Q(z,\rho), \tag{11}$$

$$T(z,\rho) = -M(z)Q(z,\rho). \tag{12}$$

Hence, by expressing $Q(z)$ as a linear combination of functions $\psi_i(z)$, each one weighted by a parameter ρ_i, *i.e.*

$$Q(z,\rho) = \psi^T(z)\rho, \tag{13}$$

where $\psi(z) = [\psi_1(z)\,\psi_2(z)\cdots\psi_n(z)]^T$, and $\rho = [\rho_1\,\rho_2\,\cdots\,\rho_n]^T$, it is possible to make both $S(z,\rho)$ and $T(z,\rho)$ affine functions of the parameter vector ρ:

$$S(z,\rho) = 1 - P(z)\psi^T(z)\rho, \tag{14}$$

$$T(z,\rho) = -M(z)\psi^T(z)\rho. \tag{15}$$

Clearly, the choice of the vector $\psi(z)$ is important. For instance, one can choose $\psi(z)$ as a collection of basis functions, through which it is possible to approximate any finite-order stable transfer function with arbitrary accuracy by increasing the value of n [26]. Among the many possible choices for defining the functions $\psi_i(z)$, in this work we considered

$$\psi_i(z) = \frac{z^{i-1}}{d(z)}, \quad i = 1,2,\ldots,n, \tag{16}$$

where the denominator $d(z)$ is a fixed polynomial of degree $n-1$. As it can be seen from Eqs. (14) and (15), the polynomial $d(z)$ determines the closed-loop poles of the considered modal

#173695 - $15.00 USD Received 2 Aug 2012; revised 12 Oct 2012; accepted 14 Oct 2012; published 16 Nov 2012

control loop. Accordingly, the choice of $d(z)$ allows to a priori fix an adequate stability margin. As will be discussed in details in Section 4, in practice $d(z)$ can be chosen on the basis of a given reference controller which represents the starting point of the proposed control design procedure.

The parameter vector ρ plays a fundamental role, in that it is used as the decision variable of the optimization problem. In fact, the objective function in Eq. (8) can be equivalently written as a quadratic function of ρ:

$$f(\rho) = \frac{1}{N}\sum_{f=1}^{N}\left\{|(1-P(e^{j\omega_f})\psi^T(e^{j\omega_f})\rho)|^2\,\hat{\Upsilon}_\phi(\omega_f) + |M(e^{j\omega_f})\psi^T(e^{j\omega_f})\rho|^2\,\hat{\Upsilon}_w(\omega_f)\right\}. \quad (17)$$

Thanks to the form of the function $f(\rho)$, it would now be immediate to compute the parameter vector, say ρ°, which minimizes $f(\rho)$. The resulting controller $C(z,\rho^\circ)$ would provide optimized performance in the sense of the minimum sampled-valued variance.

Nevertheless, in many situations a controller should fulfill additional requirements beyond stabilization and performance. For instance, while observing an astronomical object, several circumstances may cause the command signal $u(k)$ to be interrupted for a few time steps: actuators may be required to perform an action that is not compatible with its stroke or with the force they can bear (this phenomenon can be frequent, up to some events per second, in seeing conditions ≥ 1.2"); also, slopes may not be delivered for a frame or two, producing the same effects of command interruptions (though the latter is an extremely rare event).

In this respect, common practice suggests that it is not advisable to make use of unstable controllers, especially if the plant itself is stable, as it is within our setting. In fact, if the feedback loop opens (generalizing, this could happen due to a sensor or actuator failing, or deliberately being turned off during start-up or shutdown), overall stability is maintained if both plant and controller *individually* are stable ([25], Chapter 5).

Clearly, the Youla parametrization does not ensure by itself that a generic controller of the form shown in Eq. (10) is stable, thus unconstrained minimization of $f(\rho)$ can result in an unstable (albeit stabilizing) controller $C(z,\rho^\circ)$. A possible way of overcoming such a drawback consists in taking into account the controller stability requirement directly while synthesizing the controller. Accordingly, we propose to solve a *constrained* optimization problem (*COP*), defined such that $f(\rho)$ is the objective function and the controller stability requirement characterizes the feasibility domain

$$\min_{\rho} f(\rho)\,, \quad (18)$$

s.t.

$$C(z,\rho) \in \mathscr{S}. \quad (19)$$

4. Modal control design: algorithm details

Solving an optimization problem is not a trivial numerical task, and requires that the constraints, as well as the objective function, are expressed in the simplest possible form. Unfortunately, the feasibility domain embodied by Eq. (19) is in general non convex and thus it is advisable to consider some kind of convex approximation. This can be done provided that a reference parameter vector $\hat{\rho}$ is available corresponding to a stable controller $C(z,\hat{\rho})$ (in practice $\hat{\rho}$ can be computed from a given stable and stabilizing controller as will be detailed in the following). In fact, a sufficient condition for the stability of a controller $C(z,\rho)$ is that

$$Re\left\{(1-P(e^{-j\omega})Q(e^{-j\omega},\hat{\rho}))(1-P(e^{j\omega})Q(e^{j\omega},\rho))\right\} > 0\,, \qquad \forall\omega\,, \quad (20)$$

#173695 - $15.00 USD Received 2 Aug 2012; revised 12 Oct 2012; accepted 14 Oct 2012; published 16 Nov 2012

Table 1. Simulation parameters and conditions.

Telescope	diameter = 8.222 m (central obstruction 11%)
Pyramid WFS	sensing wavelength = 0.750 μm
	tilt modulation radius = $2.0\frac{\lambda}{D}$
	number of subapertures $= 30 \times 30$
	number of photons per integration time per subaperture = 213
	number of electrons per pixel of readout noise = 11.5 $e^{-}RMS$
ASM	672 Karhunen-Loève (KL) modes projected onto the ASM influence functions
turbulence	seeing $= 0.8''$ (at 0.5 μm)
	outer scale L_0 = 40 m
	mean wind speed = 16.5 m/s
telescope structural vibrations	frequencies = 13, 22 Hz
	standard deviation = 20 mas
	damping ratio = 0.01
loop parameters	sampling frequency = 1000 Hz
	2 frames total delay
Strehl Ratio calculated at	1.65 μm

where $Re\{\cdot\}$ denotes the real part. Indeed, condition in Eq. (20) ensures that the number of counterclockwise encirclements around the origin of the Nyquist plot of $1-P(z)Q(z,\rho)$ equals that of the Nyquist plot of $1-P(z)Q(z,\hat{\rho})$. In view of the Nyquist stability criterion ([27], Chapter 5), this ensures that $C(z,\rho)$ and $C(z,\hat{\rho})$ have the same stability property (recall Eq. (10)).

The condition given above is defined for all ω, *i.e.* over a continuum, thus of no practical use. One possible solution in order to avoid this drawback is to impose that Eq. (20) is satisfied only in the sampled-frequency domain $\{\omega_1,\omega_2,...\omega_N\}$. The resulting condition can be written in the form of linear constraints

$$A(\hat{\rho})\,\rho + b(\hat{\rho}) < 0 \tag{21}$$

by conveniently defining matrix A and vector b. Specifically, matrix A takes the form

$$A(\hat{\rho}) = \begin{bmatrix} a_{11}(\hat{\rho}) & \cdots & a_{1n}(\hat{\rho}) \\ \vdots & \ddots & \vdots \\ a_{N1}(\hat{\rho}) & \cdots & a_{Nn}(\hat{\rho}) \end{bmatrix} \tag{22}$$

with elements $a_{fi}(\hat{\rho})$, $f=1,...,N$, $i=1,...,n$ computed as

$$a_{fi}(\hat{\rho}) = Re\left\{(1-P(e^{-j\omega_f})Q(e^{-j\omega_f},\hat{\rho}))P(e^{j\omega_f})\psi_i(e^{j\omega_f})\right\}, \tag{23}$$

and vector $b(\hat{\rho})$ is defined as

$$b(\hat{\rho}) = [b_1(\hat{\rho})\cdots b_N(\hat{\rho})]^T \tag{24}$$

with elements $b_f(\hat{\rho})$, $f=1,...,N$ computed as

$$b_f(\hat{\rho}) = -Re\left\{1-P(e^{-j\omega_f})Q(e^{-j\omega_f},\hat{\rho})\right\}. \tag{25}$$

#173695 - $15.00 USD Received 2 Aug 2012; revised 12 Oct 2012; accepted 14 Oct 2012; published 16 Nov 2012

The problem of dealing with an infinite number of frequency constraints (as in Eq. (20)) via a finite number of frequencies has been addressed in [26] (Section 3.3), wherein guidelines on the choice of the sampled-frequency domain can be found.

Summing up, by replacing the original stability constraint in Eq. (19) with the linear constraints in Eq. (21), we obtain a quadratic programming problem which can be solved efficiently by means of several numerical tools. Typical algorithms for solving such a kind of problems are based on Active-Set, Sequential Quadratic Programming (SQM) or Interior-Point methods. In the proposed implementation, the Active-Set method has been adopted.

Herafter, we write the proposed synthesis procedure step by step and provide a schematic summary of the algorithm. As previously mentioned, the procedure starts with a pre-existing stable and stabilizing controller $\hat{C}(z)$ which can be synthesized either by means of a simple non-model based technique or of some model-based design procedure. Then we compute the Youla parameter

$$\hat{Q}(z) = \frac{\hat{C}(z)}{1+P(z)\hat{C}(z)} = \frac{\hat{n}(z)}{\hat{d}(z)} \tag{26}$$

In order to increase the degrees of freedom of our optimization problem we can introduce γ additional poles in $z=0$ and define the polynomial $d(z)$ in Eq. (16) as $d(z) = \hat{d}(z)z^{\gamma}$. Then, n is set equal to the degree of $d(z)$ increased by one, while the reference parameter vector $\hat{\rho}$ is set equal to the vector of the coefficients of the polynomial $\hat{n}(z)z^{\gamma}$. At this point, it is possible to minimize the performance criterion $f(\rho)$ under the constraints in Eq. (21). In addition, in order to improve the controller performance one can construct an iterative procedure by using, at every step, the solution of the optimization problem as a novel reference parameter vector. This idea gives rise to the following iterative procedure.

Iterative design procedure

Step 1: given an initial controller $\hat{C}(z)$ and a nonnegative integer γ, compute $d(z)$, n, and $\hat{\rho}$ as described above;
Step 2: set $i := 0$ and $\rho^{(0)} := \hat{\rho}$;
Step 3: compute the matrix $A(\rho^{(i)})$ and the vector $b(\rho^{(i)})$;
Step 4: compute the parameter vector $\rho^{(i+1)}$ as the solution of the quadratic programming problem

$$\min_{\rho} f(\rho) \tag{27}$$

s.t.

$$A(\rho^{(i)})\rho + b(\rho^{(i)}) < 0; \tag{28}$$

Step 5: if the termination criterion is met then return $\rho^{(i+1)}$; otherwise set $i := i+1$ and go back to step 3.

As for the termination criterion, we decided to impose an upper bound on the difference between the value functions corresponding to subsequent iterations, thus terminating the algorithm when $|f(\rho^{(i+1)}) - f(\rho^{(i)})| < \varepsilon$, with ε a given threshold. In this respect, notice that by construction the sequence $f(\rho^{(i)})$ is monotonically non-increasing with i. In fact, it can be easily verified that $\rho^{(i)}$ always satisfies the constraint in Eq. (28) so that $f(\rho^{(i+1)}) \leq f(\rho^{(i)})$. Since $f(\rho)$ is bounded from below, this ensures that the sequence $f(\rho^{(i)})$ converges to some finite limit and, hence, that the termination criterion is always eventually met.

#173695 - $15.00 USD Received 2 Aug 2012; revised 12 Oct 2012; accepted 14 Oct 2012; published 16 Nov 2012

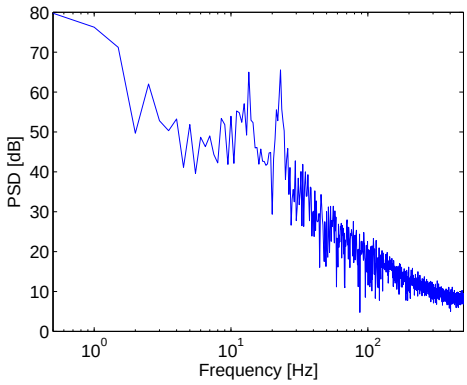

Fig. 3. Turbulence and vibration PSD related to tip.

5. Simulation results

In this section we provide the results obtained from simulation studies. The simulation results rely on an End-to-End simulator of the FLAO system. Table 1 presents a summary of the simulation parameters.

We adopted the residual phase variance and the Strehl ratio as performance parameters. Specifically, the SR is defined as

$$SR = \frac{PSF_{res}(\underline{o})}{PSF_{Airy}(\underline{o})}, \tag{29}$$

where PSF_{res} denotes the intensity value at the center $\underline{o}$ of the AO-corrected PSF and PSF_{Airy} denotes the intensity value at the center $\underline{o}$ of the diffraction-limited PSF of the telescope. The PSF_{res} is determined as the Fourier transform of the residual phase at the telescope pupil, while PSF_{Airy} is the Fourier transform of a uniform phase over the telescope pupil. The pyramid WFS [28] with tilt modulation was simulated with a full Fourier-optics code developed at the Arcetri Astrophysical Observatory. In the simulator the image on the detector is obtained by two Fourier Transforms. The first one converts, for each step of modulation, the complex amplitude of the tilted incoming wavefront into the electrical field on the pyramid; the second one converts the electrical field on the pyramid multiplied by the phase mask of the pyramid into the image on the detector. Finally the signal is computed as in [29]. The atmospheric turbulence was simulated in order to emulate a typical LBT operating environment. Specifically, the turbulent phase is represented by a set of turbulent layers, where each layer corresponds to a phase screen. In the simulations presented in this paper a set of two layers is considered. The phase screens are generated following the McGlamery method [30]. They have altitude of 0 and 6000 m over the telescope and their relative intensity is 60% and 40%, respectively (they produce a seeing of 0.8”). The temporal evolution of the turbulence is simulated, based on the Taylor’s hypothesis, by displacing the phase screens in front of the telescope pupil according to the specified speed of 15 and 18 m/s respectively. The ASM spatial response was modeled by using the influence functions determined via the FEA (Finite Elements Analysis) model of the LBT ASM, while the temporal one is considered as a delay of 1 ms. In Table 1 the simulation parameters and conditions are listed, comprising the sensor and the ASM features and the parameters characterizing the turbulence and vibrations models. Specifically, we point out that they are related to the LBT main features and typical operating conditions. Figure 3 shows the PSD of turbulence and vibrations, related to tip, as resulting from the models described in the

#173695 - $15.00 USD Received 2 Aug 2012; revised 12 Oct 2012; accepted 14 Oct 2012; published 16 Nov 2012

Table 2. Performance exhibited by the controllers considered in the simulation tests.

	$C_a(z)$	$C_b(z)$	$C_c(z)$	$C_d(z)$	$C_e(z)$	$C_f(z)$
SR %	58.51	86.22	86.49	79.20	84.02	86.61

table.

Simulation results reported hereafter consider two scenarios: in the first one, the proposed procedure is initialized from a non-model-based controller, *i.e.* from a controller synthesized without identifying mathematical models of turbulence and vibrations; in the second scenario, the proposed procedure is initialized from a H_2-controller synthesized using mathematical models of turbulence and vibrations of reduced complexity, namely a second-order AR model for the turbulence and two second-order ARMA models for the vibrations.

In both scenarios, the optimization procedure is carried out by sampling the PSDs of the phase aberration related to tip/tilt modes, as reported in Fig. 3, and the PSD of the measurement noise (assumed having variance of $\approx 10^{-4}$). As for the sampling of the PSDs in Eq. (8), we selected $N = 2000$ samples with linear gridding (simulation results, not reported here, indicate that $N > 500$ samples are sufficient for achieving satisfactory closed-loop performance). The termination criterion of the optimization algorithm was defined on the basis of the threshold $\varepsilon = 10^{-3}$ on the difference between the value functions corresponding to two successive iterations. The closed-loop performance (in terms of Strehl ratio) has been evaluated over the last 2000 samples of the residual phase (in the regime state). Finally, all the modes except for tip and tilt were controlled by means of integrators with optimized gains selected via the Optimized Modal Gain Integrator (OMGI) approach as described in [15]. Finally, also the constraint on the controller stability was considered.

First scenario: Let

$$\hat{C}(z) = \frac{gz}{z-0.95}, \tag{30}$$

with g such that the closed-loop is stable. By the procedure described in Section 4, $\hat{Q}(z)$ takes the form

$$\hat{Q}(z) = \frac{gz^2}{z^2-0.95z+g} = \frac{\hat{n}(z)}{\hat{d}(z)}. \tag{31}$$

As previously indicated, in order to increase the degrees of freedom of our optimization problem we can introduce γ additional poles in $z = 0$ and define the polynomial $d(z)$ in Eq. (16) as $d(z) = \hat{d}(z)z^{\gamma}$. Accordingly,

$$\psi_i(z) = \frac{z^{i-1}}{d(z)} = \frac{z^{i-1}}{z^{\gamma+2}-0.95z^{\gamma+1}+gz^{\gamma}}, \qquad i = 1,2,\ \ldots\ ,\ \gamma+3 \tag{32}$$

and the algorithm is then initialized by letting

$$\rho^{(0)} = \hat{\rho} = [\underbrace{0\ \ldots\ 0}_{\gamma+2}\ g]. \tag{33}$$

As for the simulation, we set $g = 0.77$. Compared with $\hat{C}(z)$, which achieves a residual phase variance (*VAR*) $VAR = 0.2528$ ($SR = 58.51\%$), Fig. 4 shows a definite performance improvement even for small values of γ, namely starting from $\gamma = 3$. In particular, for $\gamma \geq 7$ we obtain $VAR < 0.0209$ ($SR > 86.22\%$).

Second scenario: As initial controller, we now consider a H_2-controller synthesized using mathematical models of turbulence and vibrations of reduced complexity. Specifically, we adopted the design procedure described in [8], with the following choices: the model of the

#173695 - $15.00 USD Received 2 Aug 2012; revised 12 Oct 2012; accepted 14 Oct 2012; published 16 Nov 2012

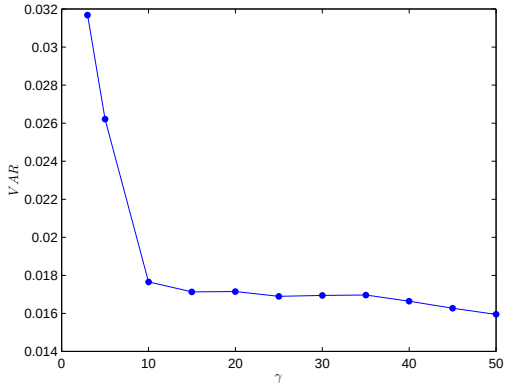

Fig. 4. Residual phase variance corresponding to controllers synthesized with increasing values of γ.

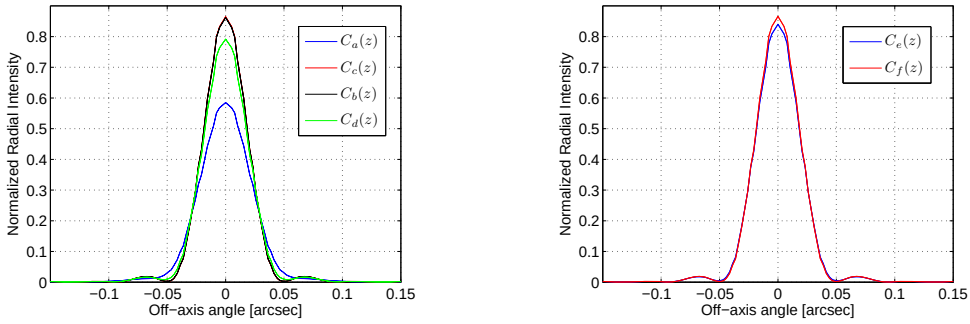

Fig. 5. PSF profiles resulting from the use of the controllers in the control loop.

turbulence is taken as a second-order AR model having input v and output ξ, and described by the difference equation

$$\xi(k) = 1.9774\,\xi(k-1) - 0.9776\,\xi(k-2) + v(k)\,, \tag{34}$$

where v is a white-noise process. As for the structural vibrations, we considered two second-order ARMA models having input μ_i and output ζ_i, $i = 1,2$. They are described by the difference equations

$$\zeta_1(k) = 1.9917\,\zeta_1(k-1) - 0.9984\,\zeta_1(k-2) + 1.8431\,\mu_1(k-1) - 0.8493\,\mu_1(k-2)\,, \tag{35}$$

for the model having a vibration peak around 13Hz, and

$$\zeta_2(k) = 1.9782\,\zeta_2(k-1) - 0.9972\,\zeta_2(k-2) + 1.7418\,\mu_2(k-1) - 0.7585\,\mu_2(k-2)\,, \tag{36}$$

for the model having a vibration peak around 22Hz, where μ_1 and μ_2 are both white-noise processes.

The order of the H_2-controller is 9 and we set $\gamma = 0$ so as to keep the order of the new controller at a moderate level. In this case, the simulation results show a performance improve-

#173695 - $15.00 USD Received 2 Aug 2012; revised 12 Oct 2012; accepted 14 Oct 2012; published 16 Nov 2012

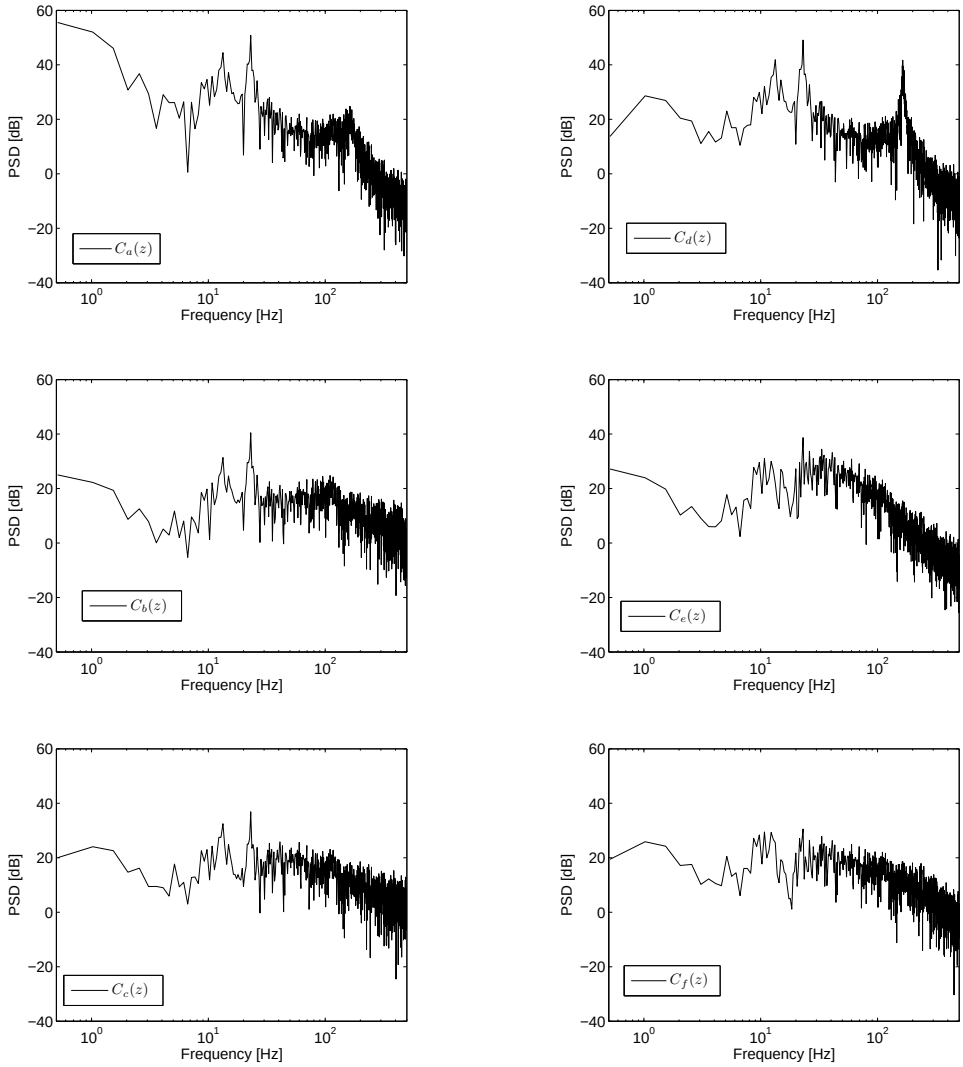

Fig. 6. PSDs of the residual phase (related to tip/tilt).

ment from $VAR = 0.0393$ ($SR = 84.02\%$) to $VAR = 0.0152$ ($SR = 86.61\%$). The performance obtained for larger values of γ is very similar to the one obtained for $\gamma = 0$.

Figures 5, 6 and 7 along with Table 2 provide a summary of the obtained results, also compared with the optimized modal gain integrator (OMGI) controller of [15], applied to all modes (including tip/tilt). For simplicity, we adopted the following notation: $C_a(z)$ initial controller in the first scenario; $C_b(z)$ final controller in the first scenario with $\gamma = 7$; $C_c(z)$ final controller in the first scenario with $\gamma = 16$; $C_d(z)$ OMGI controller; $C_e(z)$ initial controller in the second scenario; $C_f(z)$ final controller in the second scenario with $\gamma = 0$. The results are very close to what one could expect: $C_c(z)$, $C_e(z)$ and $C_f(z)$ are those exhibiting lower residual phase both at low frequencies as well as in correspondence of the vibration peaks (Fig. 6). This is also evident from Fig. 7. In particular, the sensitivity functions related to $C_e(z)$ and $C_f(z)$ both exhibit the

#173695 - $15.00 USD Received 2 Aug 2012; revised 12 Oct 2012; accepted 14 Oct 2012; published 16 Nov 2012

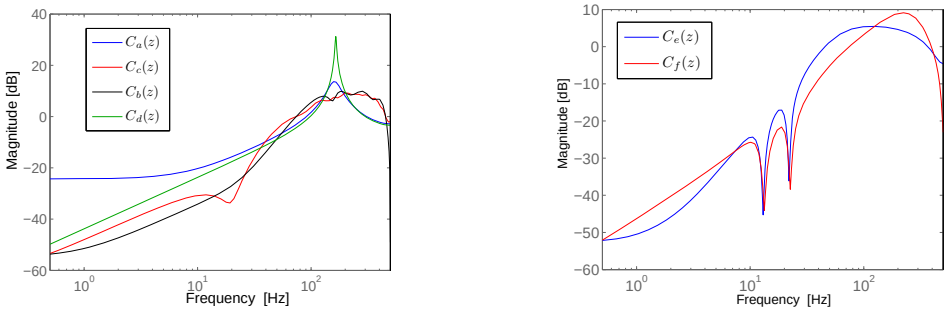

Fig. 7. Bode diagram of the sensitivity function related to the controllers.

two anti-resonance peaks at the frequencies characterizing the vibration models.

A final point is worth mentioning. One sees from Table 2 that the best peformance (considering also the order of the final controller) is achieved when starting from a model-based controller synthesized in accordance with models of reduced complexity. Such a result, obtained without identifying mathematical turbulence and vibration models of increased complexity, reinforces the idea that the proposed approach is best viewed as cooperative with (rather than as alternative to) classical AO control design approaches.

6. Conclusions

We proposed a control design technique aiming at improving the performance of AO systems using a Modal-Control approach. The basic idea relies in optimizing the Youla parameter of a given modal controller with respect to a relevant AO performance criterion defined on a sampled frequency domain. This feature makes it possible to use turbulence/vibration profiles of arbitrary complexity (even empirical PSDs from data), and can be therefore adopted to optimize: i) non-model-based controllers, avoiding any identification effort; ii) model-based controllers (such as H_2, H_∞ or LQG) synthesized in accordance with turbulence and vibration models of limited complexity. Also, the problem can be cast as a quadratic programming problem, which can be efficiently solved by means of standard optimization routines. A number of simulation results have been reported using an End-to-End Simulator of the FLAO system of the LBT. The results show that it is possible to obtain a good trade-off between performance and controller complexity by optimizing model-based controllers which are synthesized in accordance with turbulence and vibration models of reduced order. Such a feature suggests that a good trade-off can be obtained without identifying high-order turbulence and vibration mathematical models. This makes the proposed approach a promising technique to be used in combination with classical approaches to AO control design.

Several extensions are possible: most notably, the problem formulation appears flexible enough so as to take into account additional requirements which can be expressed as linear constraints within the optimization problem. For example, it is possible to impose some bounds on the sensitivity functions in order to improve robustness under perturbed conditions, thus obtaining a mixed H_2/H_∞ approach. This could be useful in the presence of system uncertainties or to deal with disturbances of intensity and/or frequency range varying with time.

#173695 - $15.00 USD Received 2 Aug 2012; revised 12 Oct 2012; accepted 14 Oct 2012; published 16 Nov 2012